Engineering Structures 266 (2022) 114553

Contents lists available at ScienceDirect

Engineering Structures

journal homepage: www.elsevier.com/locate/engstruct

Long-term viscoelastic deformation monitoring of a concrete dam: A multi-output surrogate model approach for parameter identification

Chaoning Lin [a,b], Tongchun Li [a,*], Siyu Chen [c,a,*], Li Yuan [a], P.H.A.J.M. van Gelder [d], Neil Yorke-Smith [e]

[a] College of Water Conservancy and Hydropower Engineering, Hohai University, Nanjing 210098, China
[b] College of Civil and Transportation Engineering, Hohai University, Nanjing 210098, China
[c] Nanjing Hydraulic Research Institute, Nanjing 210029, China
[d] Faculty of Technology, Policy, and Management, Delft University of Technology, Delft 2628 BX, the Netherlands
[e] Faculty of Electrical Engineering, Mathematics and Computer Science, Delft University of Technology, Delft 2628 XE, the Netherlands

ARTICLE INFO

Keywords:
Concrete dam
Inverse analysis
Surrogate model
Viscoelasticity
Multi-output Gaussian process

ABSTRACT

Dam safety monitoring has become an important topic and is critical for evaluating a dam's safety status. This study focuses on identifying the mechanical properties of a concrete dam from long-term viscoelastic deformation monitoring data. A novel inversion framework is proposed in which a surrogate model, instead of the finite element model, is placed inside the optimization loop. First, a multi-output surrogate model based on Gaussian process is trained by using data from a finite element simulation in the creep regime. In order to efficiently create a high-precision and reliable surrogate model, three test instances are conducted to investigate the impact of sample size, parameter range and output quantity on the performance of the surrogate model. Subsequently, a meta-heuristic optimization, multi-verse optimizer, is employed to identify the unknown viscoelastic parameters. The results illustrate that the identified properties allow predictions on dam displacement which are consistent with the monitoring data. Compared with the traditional inversion method based on finite element modelling, the proposed inversion method based on the multi-output surrogate model not only achieves accurate estimation of mechanical parameters but also greatly improves computational efficiency.

1. Introduction

Concrete dams play important roles in the social and economic fields by providing and facilitating flood control, power generation, water supply, and irrigation. During their service periods, dams are subjected to a variety of operational and environmental loads, and occasionally encounter some unconventional events or extreme loads (such as excessive flooding, droughts, earthquakes, etc.) [1]. Moreover, the overall performance of the concrete structures may decrease over time due to age-related deterioration, hydraulic erosion, and other factors. If a dam is not well managed and maintained, it may create a potential risk to neighbouring populations, property and environment [2].

Structural health monitoring (SHM) of concrete dams has become a topic of great importance and can help reduce the risk of dam failure through early detection of abnormality. Usually, plenty of instruments are situated inside and around the dam to monitor the water level, ambient temperature, displacement and other characteristics. Since significant amounts of data are collected from different instruments, interpretation of this data is important in SHM of concrete dams [3,4].

Data-based models is a fundamental approach in dam safety systems for both daily operation and long-term behaviour evaluation[5,6]. They are trained on previous measurements to estimate and predict the behaviour of a dam. A typical example is represented by the hydrostatic-season-time (HST) models which are widely implemented in

Abbreviations: ANNs, Artificial neural networks; DOE, Design of experiment; FEM, Finite element modelling; GP, Gaussian process; HST, Hydrostatic-season-time; LHS, Latin hypercube sampling; MOGP, Multi-output Gaussian process; MVO, Multi-verse optimizer; NLF, Negative log-likelihood function; PCE, Polynomial chaos expansion; RBF, Radial basis function; SHM, Structural health monitoring; SVR, Support vector regression; TDR, Travelling distance rate; WEP, Wormhole existence probability.

* Corresponding authors.
E-mail addresses: linchaoning@hhu.edu.cn (C. Lin), ltchhu@163.com (T. Li), sychenhhu@163.com (S. Chen), yuanli97@hhu.edu.cn (L. Yuan), P.H.A.J.M.vanGelder@tudelft.nl (P.H.A.J.M. van Gelder), N.Yorke-Smith@tudelft.nl (N. Yorke-Smith).

https://doi.org/10.1016/j.engstruct.2022.114553
Received 24 February 2021; Received in revised form 7 June 2022; Accepted 12 June 2022

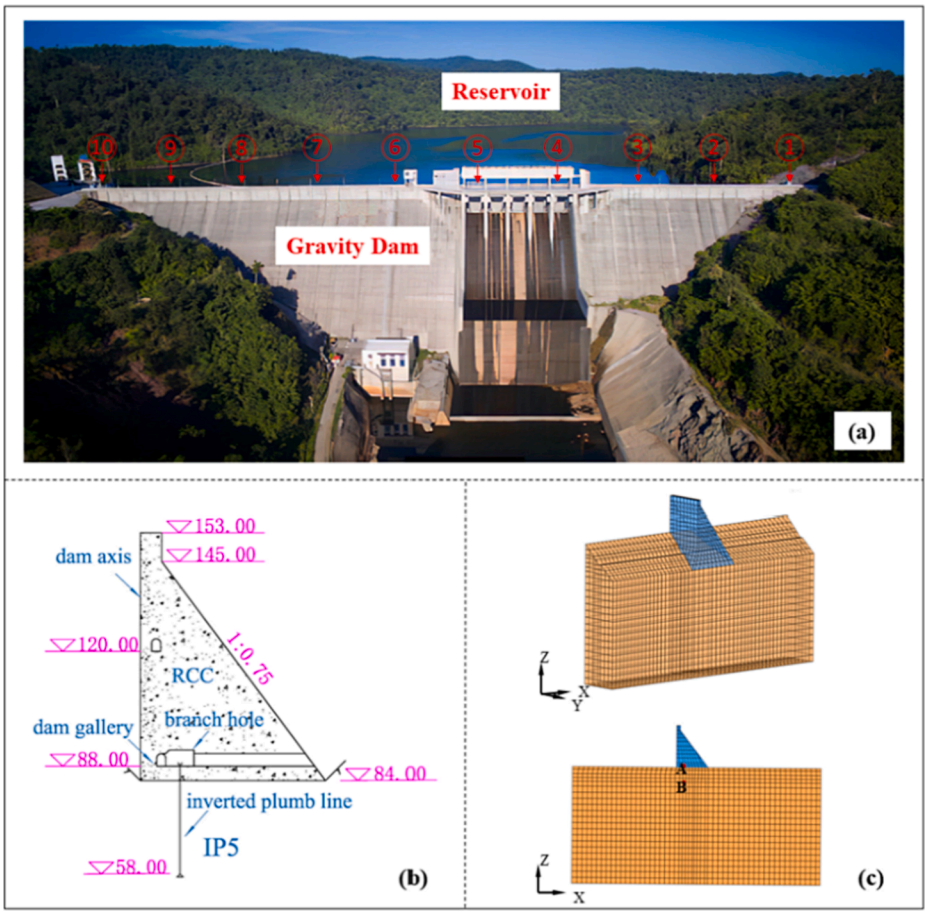

Fig. 1. (a) Photograph of the concrete gravity dam; (b) Location of IP5 in dam section #3; (c) FE mesh model of the dam section #3 and the cross section of IP5.

engineering practice. The data-based models have advantages of simplicity of formulation and efficiency of execution. However, their epitaxial prediction capability is poor. For example, it is difficult for these models to have an accurate response under conditions such as excessive flooding or earthquakes. In addition, the model parameters don't have physical meaning and these models are not able to provide an essential explanation to the dam behaviours (e.g. long-term deformation) [7,8].

Physics-based models establish relationships between loads and dam responses via structural analysis. This type of model estimates the behaviour of a dam based on information concerning material properties and physical laws governing the stress–strain relationship. However, there are few reports on the application of physics-based models to long-term dam monitoring during the operation period. There are two possible predicaments: first, the dam response, which is based on empirical parameters, results in a low prediction accuracy; second, the physics-based model is computationally inefficient because it requires an iterative analysis of a computer simulation model. Therefore, the parametric identification and further development of physics-based models are needed in the domains of dam health monitoring.

Combined with in-situ monitoring data, inverse analysis is regarded as a powerful non-destructive tool not only for identifying the mechanical parameters of dam structure [9,10], but also for the calibration of physics-based models [11]. Generally, the inverse analysis is performed by minimizing the discrepancies between calculation responses (e.g., using FE model) and measured responses, which can be formulated as an optimization problem. Due to the complex and nonlinear characteristics, it is very easy to fall into the local optimal for inverse analysis optimization problem. In the previous studies, the swarm optimizers, such as genetic algorithm [12], particle swarm optimization [13], as well as artificial bee colony algorithms [14] have been applied in dam inverse analysis, improving the precision and convergence speed of optimization. From the existing studies, it is found that most researches focused on the identification of Young modulus of the dam and its foundation as the Young modulus is a key parameter that could be used for health assessment or diagnosing of dam structure [15–18]. In fact, the creep characteristics of dam foundation and abutment are also essential for analysing dam behaviours (e.g., the long-term deformation). However, this is usually neglected by researchers.

In addition, the computational effort excessively increases when numerous simulations are required to account for the optimization in inverse analysis, especially for the situations of the large-scale numerical model and nonlinear computation. Surrogate models are a popular tool to approximate the functional relationship of expensive simulation models. Common techniques include artificial neural networks (ANNs) [19], support vector regression (SVR) [20], Gaussian process (GP) [21], polynomial chaos expansion (PCE) [22], etc. In order to address the aforementioned challenge, the surrogate models have been utilized for the purpose of reducing the computational burden in inverse analysis. Fedele et al. [23] adopted ANNs to model the non-linear relationship between input and numerical solutions, for the computing time reducing in the inversion problem of concrete dams. Dou et al. [24] established radial basis function (RBF) combined with hybrid fireworks algorithm for identifying dam parameters, verifying its superiority of computational cost reducing. Sevieri et al. [25] utilized PCE to reduce the computational burden of Bayesian updating for concrete dam parameters. Liu et al. [26] applied SVR-based inverse modelling procedure to identify the zoned elasticity modulus of an arch dam. Nevertheless, the majority of these models are generally limited to linear analysis or one-dimension output conditions, which makes applying these approaches to

Table 1
The mechanical parameters of the bedrock.

Rock type	Young modulus (GPa)	Poisson ratio	Shearing strength	Compressive strength (MPa)	Bulk density (g/cm^3)
Quartz sandstone	5 ~ 10	0.15 ~ 0.23	c = 4.7 ~ 8.4 MPa φ= 38.2° ~ 45.5°	60 ~ 80	2.5
Fine sandstone	7 ~ 8	0.18 ~ 0.25	c = 3 ~ 5 MPa φ= 35° ~ 45°	45 ~ 55	2.5
Silty mudstone	2 ~ 3	0.28 ~ 0.30	c = 0.8 ~ 1.0 MPa φ = 35° ~ 38°	10 ~ 20	2.5
Mudstone	1 ~ 2	0.30 ~ 0.35	c = 0.6 ~ 0.8 MPa φ = 30° ~ 35°	1 ~ 3	2.4

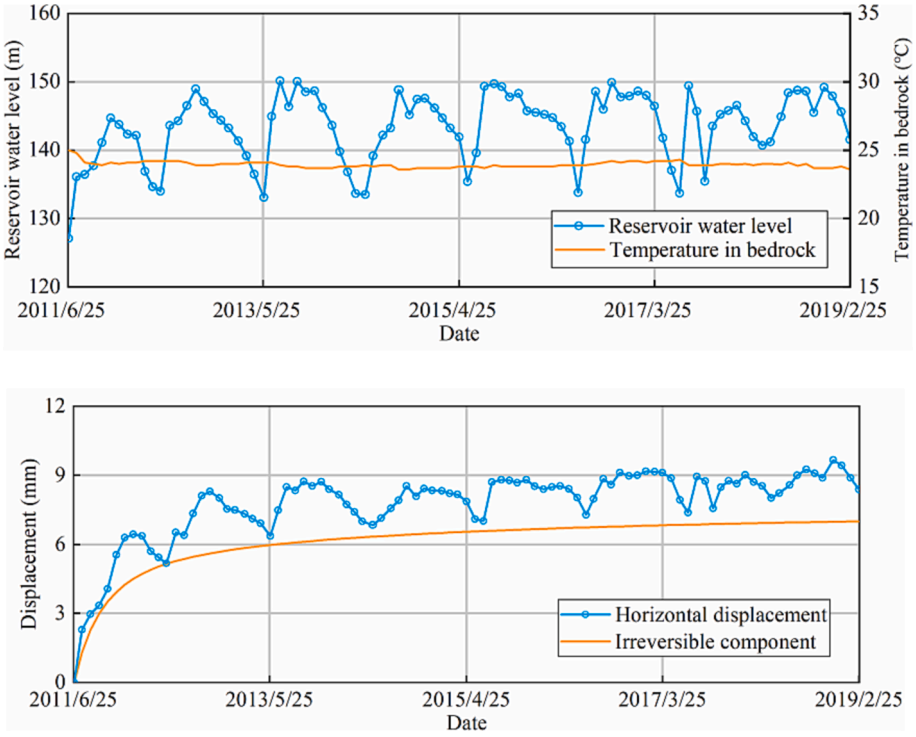

Fig. 2. Displacement monitored by inverted plumb line IP5 plotted with the reservoir water level and temperature in the dam foundation.

nonlinear and multi-output inverse analysis intractable.

Gaussian process (GP) has emerged as one of the most popular surrogate modelling techniques and powerful approximator [27]. In the past, GP was adopted in the field of engineering structure, such as structural response prediction [28–31], structural reliability analysis [32,33] and model updating [34]. Typical GP is usually designed for single-output scenarios wherein the output is a scalar. The extension from single- to multi-output Gaussian process (MOGP) model is motivated by the problem of approximating multiple outputs simultaneously. MOGP provide a flexible framework for probabilistic regression and has been used to solve many high-dimensional, small sample size and nonlinear problems [35–37]. In comparison with NNs, SVR and other conventional surrogate techniques, MOGP is simple to implement, flexible and self-adaptive in the determination of hyperparameters. In addition, MOGP is descriptive to incorporate information from learning processes and capture complex relationships between multi-input and multi-output variables [38].

In general, the long-term deformation of concrete dams is a very common phenomenon. Some dams exhibit obvious irreversible deformation over the operation period due to the creep of dam bedrock. This work aims to solve two issues: (1) establish a surrogate model-based inversion framework to identify multiple viscoelastic parameters in an accurate and efficient manner, and (2) predict the long-term deformation characteristic of the dam using a physics-based model with calibrated parameters. The case study is a concrete dam located in Cambodia that has been gradually deformed over its operation period [39]. The Burgers constitutive model is applied to fit the creep data and to describe the viscoelastic properties of the dam foundation. To handle the computational burden of inverse analysis, a novel inversion method is proposed which incorporate surrogate modelling and *meta*-heuristic optimization techniques. The MOGP model is placed within the search loop to approximate parameters of the constitutive model of dam system. The performance of the MOGP model is highly dependent on the sample size, parameter range and output quantity. In order to improve the efficiency of MOGP, a series of test instances are executed and some insightful details are provided. Moreover, the research also verifies the rationality of the physics-based monitoring model based on calibrated parameters.

The remainder of this article is organized as follows. In Section 2, the operation situation of a concrete gravity dam case in Cambodia are reviewed, and the numerical model is described. In Section 3, the developed inversion method based on the MOGP surrogate model is introduced. In Section 4, a series of empirical tests and analyses are performed on a dam section to verify the effectiveness of the proposed inversion method. Further, this section discusses and highlights the advantages of the proposed method, which differ from current inversion

methods of concrete dams. Finally, in Section 5, concluding remarks and future directions are provided.

2. Project background

The case study is a concrete gravity dam located in Cambodia (Fig. 1 (a)). The elevation of the dam crest is at 153 m asl (above sea level); the foundation surface is at 41 m asl, with a maximum dam height of 112 m. A monitoring system was installed to monitor the dam status. The measured items include reservoir water levels, air temperatures, displacements, seepage and so on. The monitoring data indicate that the dam has been gradually deformed over the operation period (2011–2019), and the creep effect of the dam bedrock is significant.

2.1. Hydrological and geological conditions

The first impoundment of the project was in April 2011. After that, the upstream water level rose between 133 m asl and 150 m asl. The average monthly temperature in the reservoir area varies between 25.0℃ and 28.4℃; the mean temperature is 26.9℃. The dam bedrock is mainly composed of quartz sandstone and fine sandstone, with silty mudstone and mudstone interbeds. The material properties of the bedrock were determined by tests. The mechanical parameters with a 95% confidence interval are presented in Table 1, where c represents the cohesion and φ represents the internal friction angle.

2.2. Data description

The dam has a total of ten dam sections and is equipped with eight inverted plumb lines for monitoring the displacement of the dam foundation in the upstream–downstream direction. The inverted plumb line (Fig. 1(b)) is installed in the bottom gallery of the dam. The lower end of the plumb line is fixed at 58 m asl, and the upper end is linked to a float submerged in a water box in the observation area (88 m asl). The length of the plumb line is 30 m.

The observed data of the inverted plumb line show that the deformation of the dam foundation in the upstream–downstream direction has an increasing trend during the operation period. We take dam section #3 as a representative example in this study. Fig. 2 shows the time history curve of environmental variables and corresponding horizontal displacement responses of the inverted plumb line IP5 in section #3. The temperature curve in Fig. 2 is measured by a representative thermometer situated near the IP5 (65 m asl, 14 m down the dam axis). Observations are recorded monthly from June 25, 2011, to February 25, 2019, for a total of 93 measurements.

The measured displacement of the dam foundation is composed of the reversible component and the irreversible component. It can be seen from Fig. 2 that the crests and troughs of the displacement closely correlate with the reservoir water level. The temperature in the dam foundation is stable according to the measurements of the thermometers. It is deduced that the reservoir water level is the main reason for the reversible component. The irreversible component, which is caused by time-dependent deformation of the dam foundation, can be separated via HST statistical model and multiple least square regression procedure [39], and the obtained irreversible component is shown in Fig. 2. During the years from 2011 to 2019, the irreversible component is 7 mm towards the downstream direction, accounting for about 80% of the total displacement; the irreversible component tends to be stable in recent years.

2.3. Finite element modelling

To understand the monitoring results and analyse the behaviour of the dam foundation, a numerical model is established. Viscoelasticity is used to describe the stress–strain-time relation of time-dependent materials. A widely-used four-parameter Burgers model is adopted in this study. The constitutive model can be regarded as the combination of the Maxwell model and Kelvin model [40]. The constitutive equations are as follows:

$$\begin{cases} \sigma_{\mathrm{M}} = E_{\mathrm{M}}\varepsilon_{\mathrm{M}} = \eta_{\mathrm{M}}\dot{\varepsilon}_{\mathrm{M}} \\ \sigma_{\mathrm{K}} = E_{\mathrm{K}}\varepsilon_{\mathrm{K}} + \eta_{\mathrm{K}}\dot{\varepsilon}_{\mathrm{K}} \\ \sigma = \sigma_{\mathrm{M}} = \sigma_{\mathrm{K}} \\ \varepsilon = \varepsilon_{\mathrm{M}} + \varepsilon_{\mathrm{K}} \end{cases} \tag{1}$$

where σ and ε represent the stress and strain;σ_{M}, ε_M and $\dot{\varepsilon}_M$ are the stress, strain, and strain rate of the Maxwell body, respectively;σ_K, ε_K and $\dot{\varepsilon}_K$ are the stress, strain, and strain rate of the Kelvin body, respectively; E_M and η_M denote the elastic modulus and viscosity coefficient of the Maxwell body; E_K and η_K denote the elastic modulus and viscosity coefficient of the Kelvin body.

Using the Laplace transform to solve Eq. (1), the corresponding creep constitutive equation can be obtained. Eqs. (2) and (3) show the one-dimensional and three-dimensional creep equations of the Burgers model, respectively.

$$\varepsilon = \frac{\sigma}{E_M} + \frac{\sigma}{\eta_M}t + \frac{\sigma}{E_K}\left[1 - \exp\left(-\frac{E_K}{\eta_K}t\right)\right] \tag{2}$$

$$e_{ij} = \frac{S_{ij}}{2G_M} + \frac{S_{ij}}{2\eta_M}t + \frac{S_{ij}}{2G_K}\left[1 - \exp\left(-\frac{G_K}{\eta_K}t\right)\right] \tag{3}$$

where S_{ij} and e_{ij} represent the deviatoric stress and strain, respectively; G_M denotes the shear modulus of the Maxwell body; G_K denotes the shear modulus of the Kelvin body under three-dimensional conditions.

Under the action of loads P, the relationship between the structural displacement and mechanical parameters of the Burgers model is the following:

$$y_t' = f(E_M, E_K, \eta_M, \eta_K, \nu, t, P) \tag{4}$$

where y_t' is the displacement response at the time$t$; and ν denotes the Poisson ratio.

A 3D FE model of the dam section #3 was carried out according to the actual situation of the measuring points, as shown in Fig. 1 (c). The model simulates a domain of dam foundation with about 2.0 times the maximum dam height both upstream and downstream, and about 2.0 times the maximum dam height beneath the dam bottom. The FE mesh includes 9,181 eight-node hexahedral elements and 10,789 nodes. The element size was determined via convergence analysis. The lower and upper ends of the inverted plumb line IP5 are represented by nodes A and B in the cross section of Fig. 1(c), respectively.

The described model was implemented by GeHoMadrid, a FE program that was jointly developed between Technical University of Madrid (Spain) and Hohai University (China) [41]. The program is developed in Fortran and incorporates the PARDISO package for solving highly complicated and sparse equations. It is commonly used to solve complex structural, fluid and multi-physics problems in geotechnical and hydraulic engineering [42].

In FE simulation, the side faces of the dam foundation are subject to normal constraints, and the nodes at the bottom boundary are spatially fixed. The dam concrete is simulated by the elastic model and the bedrock is simulated by the Burgers model. The dam foundation has crept under its deadweight for several years. Then the weight of the concrete dam body is loaded stepwise and the upstream hydrostatic pressure is applied according to water storage conditions. Hence, the step analyses start from the initial time (June 25, 2011), and the calculation interval is one month. The FE analysis determines the relative displacement between nodes A and B, which corresponds to the measured value of IP5. After deducting the initial displacement, the displacement values obtained in the subsequent calculation can be compared with the measured displacements.

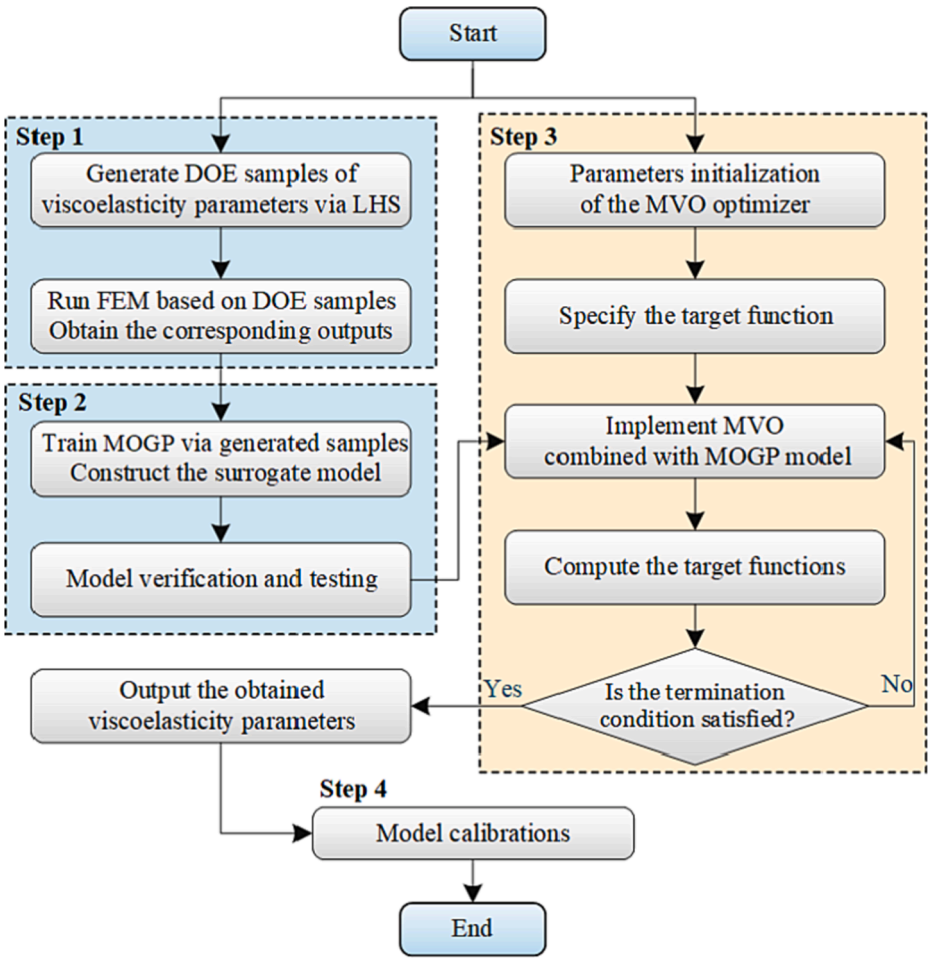

Fig. 3. Flowchart of the inverse analysis framework.

3. Methodology

In this section, the proposed inversion method of mechanical parameters is introduced. The approach consists essentially of three parts: (1) the construction of the MOGP surrogate model for a fast calculation of viscoelastic displacement responses of the dam; (2) the formulation of an objective function (or error function) measuring the difference between model responses and monitoring results; and (3) the selection of an optimization strategy to enable the search for the minimum of the objective function.

3.1. Overview of the proposed inversion framework

Fig. 3 gives a graphical flowchart for the proposed inversion framework. Four main steps are summarized as follows:

Step 1: Data preparation and finite element computation

In order to extract the maximum amount of information, design of experiment (DOE) techniques are employed to determine the input samples $\mathbf{X} \in R^{N\times d}$, where N is the number of design points and d is the dimension of the input variables. In this study, the input variables are the viscoelastic parameters of the Burgers model to be identified. The Latin hypercube sampling (LHS) method [43] is applied to uniformly generate N pairs of parameter samples within their ranges. The input samples are transferred to the FE program to calculate corresponding dam displacement responses at different times, yielding a set of vector outputs $\mathbf{Y} \in R^{N\times T}$, where T is the number of the outputs. Finally, the inputs-outputs dataset $\mathbf{D} = [\mathbf{X}, \mathbf{Y}]$ can be obtained.

Step 2: MOGP model construction

The initial dataset $\boldsymbol{D} = [\mathbf{X}, \mathbf{Y}]$ is split into two parts: training set and testing set. A MOGP model is constructed to map the relationship between input parameters and output dam responses. An introduction of MOGP modelling is provided in Section 3.2. Section 3.2 also introduces the performance criteria on the training/testing set to verify whether the trained MOGP model has acceptable prediction accuracy. When the MOGP model performs well in the testing set, the trained MOGP model can be used as a surrogate model to replace the FE model.

Step 3: Objective function formulation and parameter identification

The parameter inversion problem is converted into an optimization problem of an objective function (Section 3.3). The objective function that evaluates the error between the model responses and monitoring results is specified and then minimized, in which the viscoelastic parameters play the role of the variables to be optimized. In particular, we adopt the multi-verse optimizer (MVO) to conduct the optimization process and identify the unknown parameters (Section 3.3).

Step 4: Model calibrations

To verify the reliability of the proposed inversion method, the forward method is used to calculate the displacement of the dam based on the identified parameters. The root mean square error (*RMSE*) is employed for evaluating the fitted and predicted performance of the dam displacements based on the inversion results.

3.2. MOGP surrogate model

The input of the surrogate model is the viscoelastic parameters of the Burgers model, and the output is the relative displacement between the

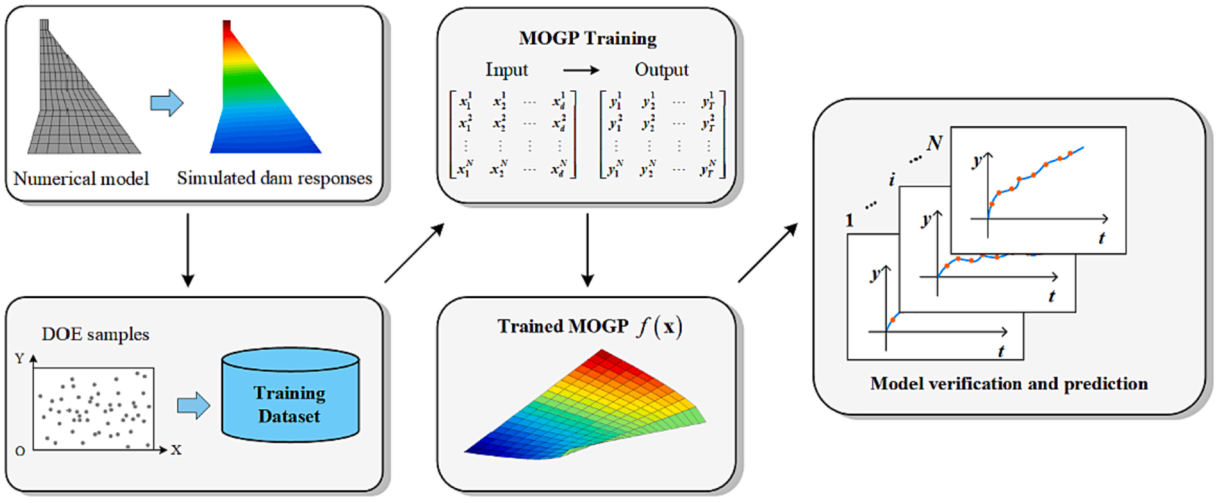

Fig. 4. Flowchart of MOGP surrogate model for dam response prediction.

Table 2
$L_9(3^4)$ orthogonal test.

Test number	A (E_M)	B (E_K)	C (η_M)	D (η_K)	Factors and levels of experiment design				Results
					E_M (GPa)	E_K (GPa)	η_M (GPa·year)	η_K (GPa·year)	$F(X)$ (mm^2)
1	1	1	1	1	1	1	50	1	307.91
2	1	2	2	2	1	3	100	3	23.75
3	1	3	3	3	1	5	150	5	5.72
4	2	1	2	3	3	1	100	5	36.97
5	2	2	3	1	3	3	150	1	0.61
6	2	3	1	2	3	5	50	3	0.96
7	3	1	3	2	5	1	150	3	65.01
8	3	2	1	3	5	3	50	5	1.55
9	3	3	2	1	5	5	100	1	6.41

Table 3
Mean value of each factor in correspondence with levels.

	E_M	E_K	η_M	η_K
K_1	112.46	136.63	103.47	104.98
K2	12.84	8.64	22.38	29.91
K3	24.32	4.36	23.78	14.75
R	99.62	132.27	81.10	90.23

nodes at the position of the inverted plumb line (Fig. 1(c)), which corresponds to the measured value of IP5. It is assumed that a set of simulation data $\mathbf{D} = [\mathbf{X}, \mathbf{Y}]$ is collected at N input samples of d-dimensional viscoelastic parameters $\mathbf{x} = [x_1, \ldots, x_d]$ from the original FE model. $\mathbf{Y}$ is an $N \times T$ output matrix and the i-th row of the response $\mathbf{Y}$ contains the quantities of$\mathbf{y}^i = [y_1^i, \ldots, y_T^i]$, where T is the number of the displacement time-series data. Since all displacement time-series data depend on the realization of the viscoelastic parameters $\mathbf{x}$, it is a typical multi-input and multi-output problem. The task of GP modelling is the establishment of a functional relationship between the parameters $\mathbf{X}$ and displacement responses $\mathbf{Y}$.

$$\mathbf{Y} = f(\mathbf{X}) \tag{5}$$

where $\mathbf{X} = [\mathbf{x}^1, \mathbf{x}^2, \ldots, \mathbf{x}^N]^T$ contains n realization of parameters; $\mathbf{Y} = [\mathbf{y}^1, \mathbf{y}^2, \ldots, \mathbf{y}^N]^T$ are corresponding responses.

Table 4
The average training/testing errors of the MOGP model in ten runs (unit: mm).

Size	Training					Testing				
	aRMSE	*MAXE*	*aMAE*	aR^2	Time(s)	*aRMSE*	*MAXE*	*aMAE*	aR^2	Time(s)
20	0.221	0.824	0.123	0.997	2.4	1.482	4.151	1.066	0.882	0.8
30	0.175	0.569	0.119	0.998	2.5	1.118	3.375	0.778	0.928	0.8
40	0.156	0.643	0.081	0.998	2.7	1.084	3.391	0.739	0.934	0.9
50	0.160	0.861	0.072	0.999	2.8	0.890	3.209	0.606	0.954	0.9
60	0.264	1.204	0.166	0.996	3.0	0.847	3.578	0.571	0.957	0.9
70	**0.430**	**1.654**	**0.301**	**0.990**	**3.1**	**0.789**	**2.305**	**0.543**	**0.964**	**0.9**
80	**0.633**	**2.242**	**0.448**	**0.981**	**3.1**	**0.829**	**3.637**	**0.561**	**0.959**	**1.0**
90	**0.723**	**2.702**	**0.508**	**0.970**	**3.2**	**1.026**	**4.413**	**0.664**	**0.946**	**1.0**
100	**0.834**	**3.063**	**0.584**	**0.962**	**3.5**	**1.101**	**4.978**	**0.734**	**0.934**	**1.1**
125	1.017	3.780	0.740	0.938	3.8	1.212	5.250	0.837	0.910	1.2
250	1.457	6.622	1.061	0.880	6.0	1.510	6.774	1.092	0.859	1.6
500	1.541	7.434	1.099	0.867	31.4	1.539	6.927	1.103	0.862	6.2
750	1.493	8.468	1.058	0.873	64.3	1.500	8.396	1.062	0.867	13.1
1000	1.441	7.542	1.025	0.880	116.2	1.501	8.037	1.057	0.877	22.5

Table 5
The standard deviation of training/testing errors of the MOGP model in ten runs (unit: mm).

Size	Training				Testing			
	aRMSE	*MAXE*	*aMAE*	aR^2	*aRMSE*	*MAXE*	*aMAE*	aR^2
20	0.081	0.376	0.035	0.002	0.297	1.356	0.170	0.049
30	0.031	0.159	0.018	0.001	0.212	0.919	0.101	0.017
40	0.063	0.283	0.028	0.002	0.151	0.891	0.062	0.017
50	0.054	0.370	0.015	0.001	0.107	0.590	0.054	0.013
60	0.046	0.412	0.019	0.002	0.116	0.904	0.060	0.011
70	**0.042**	**0.287**	**0.029**	**0.002**	**0.127**	**0.786**	**0.081**	**0.007**
80	**0.046**	**0.399**	**0.035**	**0.002**	**0.134**	**0.802**	**0.081**	**0.008**
90	**0.048**	**0.407**	**0.036**	**0.003**	**0.129**	**0.922**	**0.085**	**0.010**
100	**0.031**	**0.248**	**0.032**	**0.003**	**0.105**	**0.294**	**0.045**	**0.009**
125	0.051	0.415	0.040	0.006	0.131	0.679	0.069	0.011
250	0.044	0.763	0.032	0.006	0.084	0.925	0.047	0.011
500	0.034	0.406	0.029	0.004	0.076	0.922	0.040	0.007
750	0.022	0.546	0.015	0.003	0.048	0.753	0.023	0.006
1000	0.020	0.969	0.024	0.003	0.051	0.829	0.026	0.005

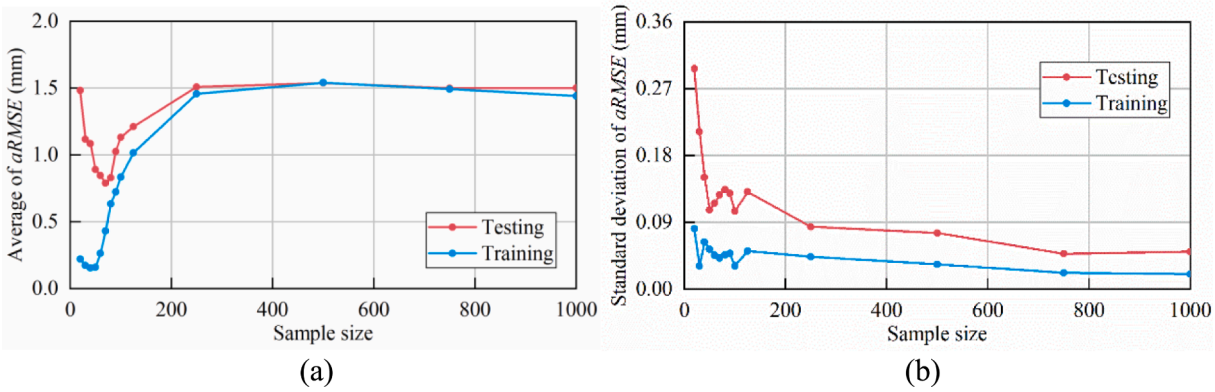

Fig. 5. The training/testing errors of the MOGP model under different sample size (the original input parameter range and 93 output observations): (a) Average of *aRSME*; (b) Standard deviation of *aRSME*.

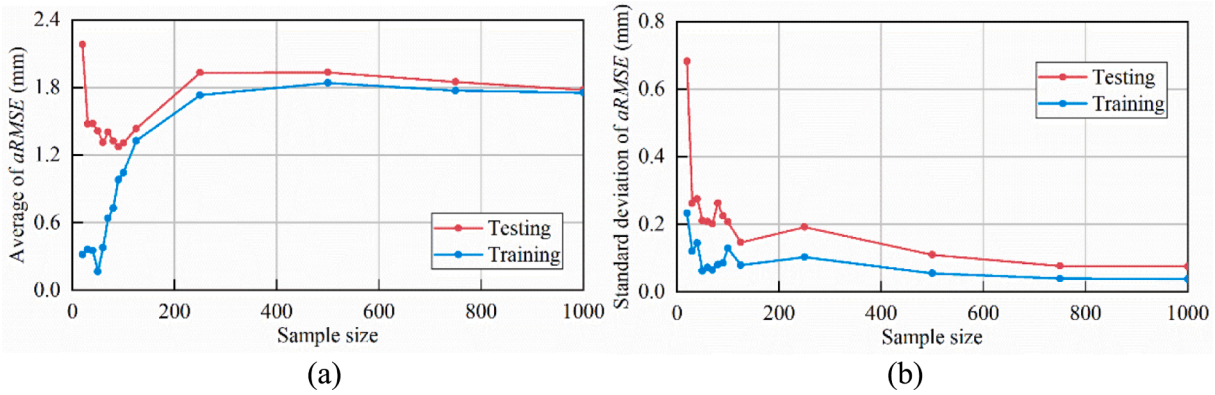

Fig. 6. The training/testing errors of the MOGP model under different sample size (the expanded input parameter range and 93 output observations): (a) Average of *aRSME*; (b) Standard deviation of *aRSME*.

3.2.1. *Multi-output Gaussian process*

An introduction to the MOGP models is provided below [27]. In many realistic scenarios, we only have the observation of the exact function value as:

$$y_t(\mathbf{x}) = f_t(\mathbf{x}) + \varepsilon_t, \varepsilon_t \sim N\left(0, \sigma_{s,t}^2\right) \tag{6}$$

where ε_t represents the additive white noise assigned to the t-th output. It is assumed that ε_t is independent and subjected to a Gaussian distribution with a mean of zero and a variance of $\sigma_{s,t}^2$.

The T target outputs $\boldsymbol{f}(\mathbf{x}) = \{f_1(\mathbf{x}), \ldots, f_T(\mathbf{x})\}^{\mathrm{T}}$ are assumed to follow a Gaussian process as:

$$f(\mathbf{x}) \sim gp(\mathbf{0}, \mathbf{k}_M(\mathbf{x}, \mathbf{x}^{'})) \tag{7}$$

where $\mathbf{x}, \mathbf{x}^{'} \in \mathbf{X}$ are d-dimensional input vectors; the multi-output covariance $\mathbf{k}_M(\mathbf{x}, \mathbf{x}^{'}) \in R^{T\times T}$ is defined as:

$$\mathbf{k}_M(\mathbf{x}, \mathbf{x}^{'}) = \begin{bmatrix} k_{11}(\mathbf{x}, \mathbf{x}^{'}) & \cdots & k_{1T}(\mathbf{x}, \mathbf{x}^{'}) \\ \vdots & \ddots & \vdots \\ k_{T1}(\mathbf{x}, \mathbf{x}^{'}) & \cdots & k_{TT}(\mathbf{x}, \mathbf{x}^{'}) \end{bmatrix} \tag{8}$$

The matrix element $k_{tt^{'}}(\mathbf{x}, \mathbf{x}^{'})(t = 1, \cdots, T)$ represent the covariance/

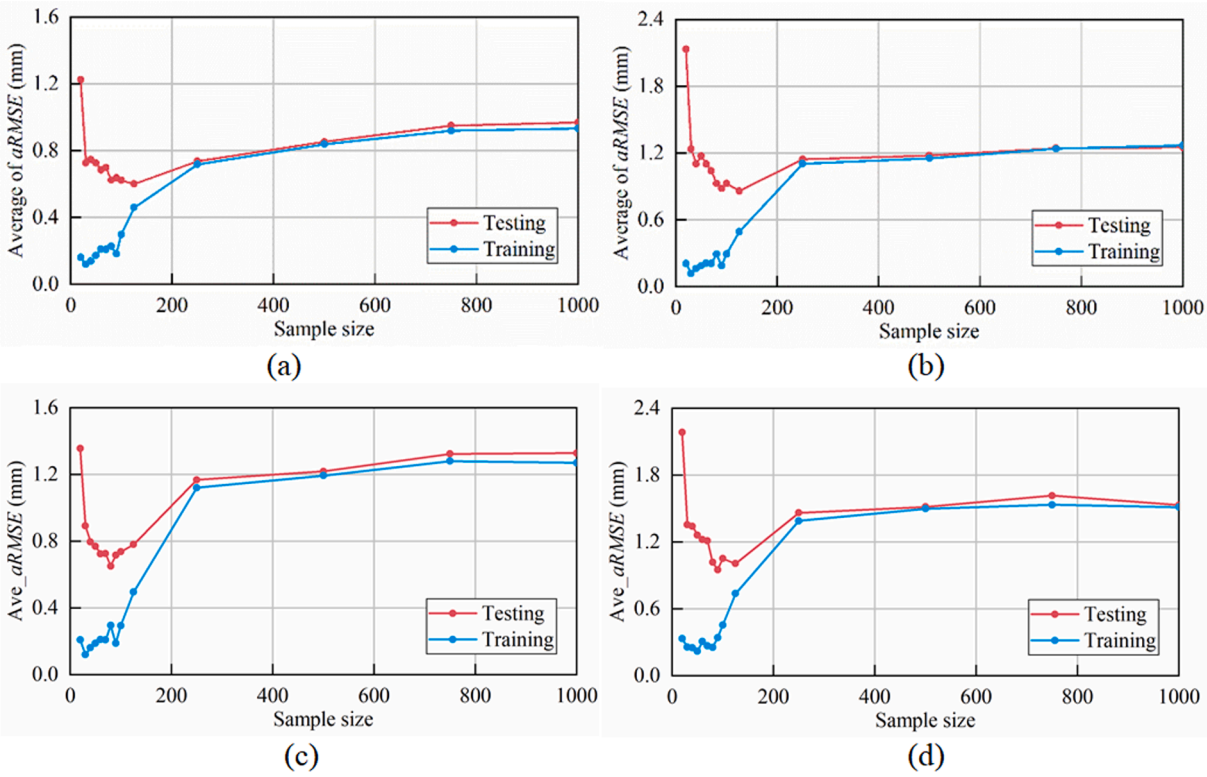

Fig. 7. The average of *aRSME* of the MOGP model under different sample size: (a) the original input parameter range and 30 output observations; (b) the expanded input parameter range and 30 output observations; (c) the original input parameter range and 60 output observations; (d) the expanded input parameter range and 60 output observations.

correlation between outputs $f_t(\mathbf{x})$ and $f_{t'}(\mathbf{x})$. One frequently used example of the covariance function is the squared exponential covariance function:

$$k_{SE}(\mathbf{x},\mathbf{x}') = \sigma_f^2 \exp\left(-\frac{1}{2l^2}(\mathbf{x}-\mathbf{x}')^T(\mathbf{x}-\mathbf{x}')\right) \tag{9}$$

where the signal variance σ_f^2 represents an output scale amplitude; the characteristic length scale l represents the correlation size associated with the differences among inputs.

The likelihood function for the T outputs follows:

$$p(\mathbf{y}|\mathbf{f},\mathbf{x},\boldsymbol{\Sigma}_s) = \mathcal{N}(\mathbf{f}(\mathbf{x}),\boldsymbol{\Sigma}_s) \tag{10}$$

where $\boldsymbol{\Sigma}_s \in R^{T\times T}$ is a diagonal matrix with the element $\left\{\sigma_{s,t}^2\right\}_{1\leqslant t\leqslant T}$.

Then given the training set $\mathbf{D} = [\mathbf{X},\mathbf{Y}]$ and testing points $\mathbf{X}_*$, the joint posterior distribution over $\mathbf{Y}_*$ can be expressed as:

$$p(\mathbf{Y}_*|\mathbf{X},\mathbf{Y},\mathbf{X}_*) \sim N(m(\mathbf{Y}_*), var(\mathbf{Y}_*)) \tag{11}$$

The mean and covariance of $\mathbf{Y}_*$ take the following form:

$$m(\mathbf{Y}_*) = \mathbf{K}_M(\mathbf{X},\mathbf{X}_*)^T[\mathbf{K}_M(\mathbf{X},\mathbf{X}) + \boldsymbol{\Sigma}_M]^{-1}\mathbf{Y} \tag{12}$$

$$var(\mathbf{Y}_*) = \mathbf{K}_M(\mathbf{X}_*,\mathbf{X}_*) - \mathbf{K}_M(\mathbf{X},\mathbf{X}_*)^T[\mathbf{K}_M(\mathbf{X},\mathbf{X}) + \boldsymbol{\Sigma}_M]^{-1}\mathbf{K}_M(\mathbf{X},\mathbf{X}_*) \tag{13}$$

where $\mathbf{K}_M(\mathbf{X},\mathbf{X}) \in R^{nT\times nT}$ is the symmetric and block partitioned matrix with the block $\mathbf{K}_{tt'}(\mathbf{X},\mathbf{X}) \in R^{n\times n}(t,t' = 1,\cdots,T)$; similarly, $\mathbf{K}_M(\mathbf{X},\mathbf{X}_*) \in R^{nT\times pT}$ has the block $\mathbf{K}_{tt'}(\mathbf{X},\mathbf{X}_*) \in R^{n\times p}$ and $\mathbf{K}_M(\mathbf{X}_*,\mathbf{X}_*) \in R^{pT\times pT}$ has the block $\mathbf{K}_{tt'}(\mathbf{X}_*,\mathbf{X}_*) \in R^{p\times p}$; $\boldsymbol{\Sigma}_M = \boldsymbol{\Sigma}_s \otimes \mathbf{I}_n \in R^{nT\times nT}$ is a diagonal noise matrix.

Before using Eq. (12) and (13) to make a prediction, we need to infer the hyperparameters $\boldsymbol{\theta}_M$ of the MOGP model. The hyperparameters $\boldsymbol{\theta}_M$ include the parameters in the covariance function and the noise process (i.e. parameters in $\{\mathbf{K}_{tt'}\}_{1\leqslant t,t'\leqslant T}$ and $\left\{\sigma_{s,t}^2\right\}_{1\leqslant t\leqslant T}$ for the T outputs), which can be learned by minimizing the negative log-likelihood function (NLF) based on the training data:

$$\boldsymbol{\theta}_M^{opt} = \left\{\sigma_{f,t}^{opt},\ l_t^{opt},\ \sigma_{s,t}^{opt}\right\}_{1\leqslant t\leqslant T} = \underset{\boldsymbol{\theta}_M}{\operatorname{argmin}} NLF \tag{14}$$

where.

$$NLF = -\log p(\mathbf{y}|\mathbf{X},\boldsymbol{\theta}) = \frac{1}{2}\mathbf{y}^T\left[\mathbf{K}(\mathbf{X},\mathbf{X}) + \sigma_n^2\mathbf{I}_n\right]^{-1} + \frac{1}{2}\log\left|\mathbf{K}(\mathbf{X},\mathbf{X}) + \sigma_n^2\mathbf{I}_n\right| + \frac{n}{2}\log 2\pi \tag{15}$$

The optimal hyperparameters $\boldsymbol{\theta}_M^{opt}$ can be solved by utilizing the conjugate gradient algorithm after parameter initialization [44].

3.2.2. Performance criteria of the MOGP model

Fig. 4 gives a graphical flowchart for MOGP modelling. The MOGP surrogate model is trained by the input–output samples generated by FE experiments. Before using it to make inference on the original simulator output, the performance of the trained MOGP model should be evaluated quantitatively. The metrics used in this study include the average root mean square error (*aRMSE*), maximum absolute error (*MAXE*), average mean absolute error (*aMAE*), and average coefficient of determination (aR^2), which are expressed as follows:

$$aRMSE = \frac{1}{T}\sum_{j=1}^{T}\sqrt{\frac{1}{N}\sum_{i=1}^{N}(f_{ij}-y_{ij})^2} \tag{16}$$

$$MAXE = \max\left|f_{ij}-y_{ij}\right| \tag{17}$$

$$aMAE = \frac{1}{T}\sum_{j=1}^{T}\frac{1}{N}\sum_{i=1}^{N}\left|f_{ij}-y_{ij}\right| \tag{18}$$

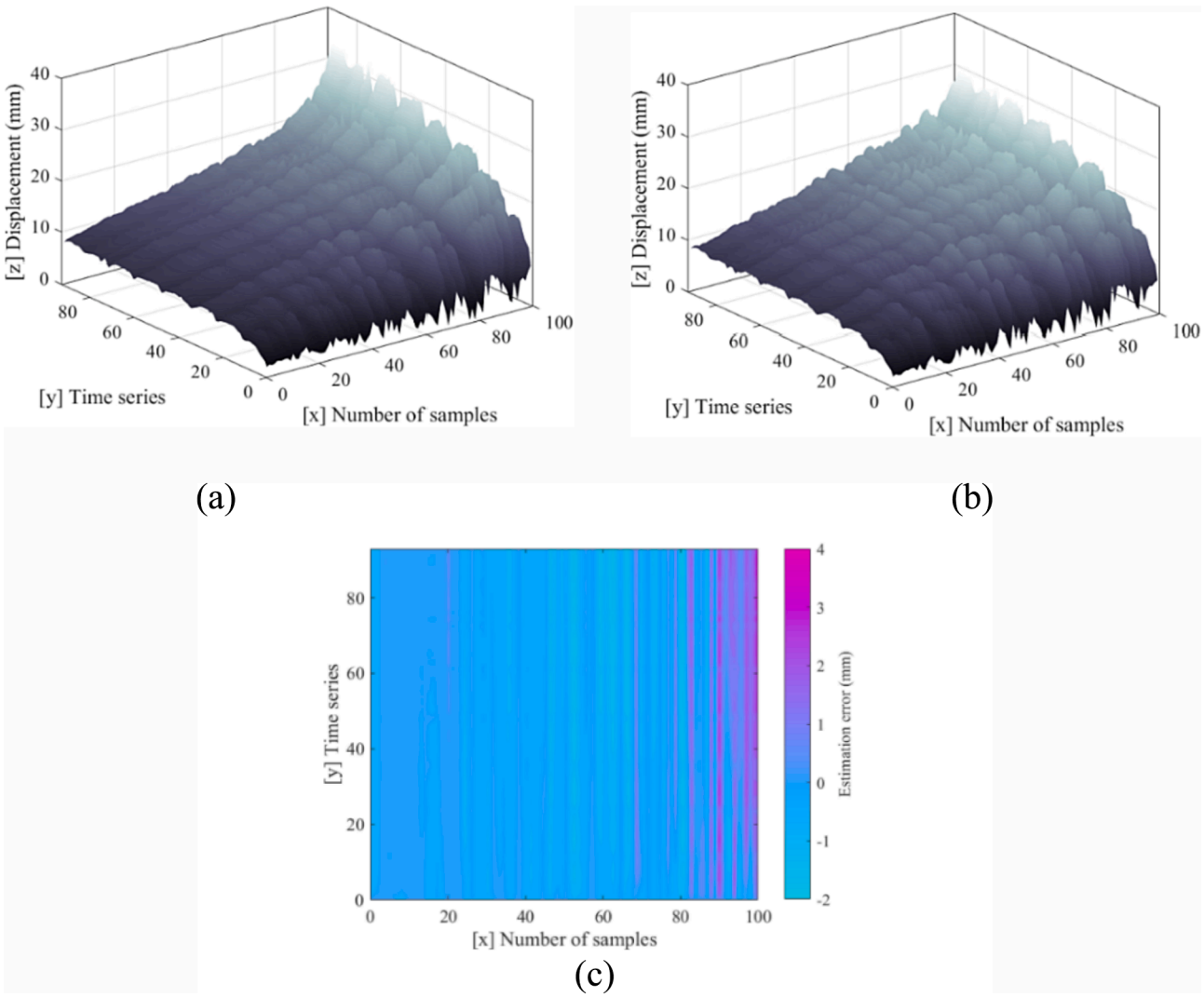

Fig. 8. The performance evaluation of the MOGP surrogate model: (a) response surface of FE model; (b) response surface of MOGP model; (c) estimation error between FE model and MOGP model.

Table 6
Comparison of the optimal objective-function value and the computational time.

Model	Minimum (best)	Maximum (worst)	Average	Standard deviation	Computational time (s)
MOGP model I	3.1580	3.3323	3.2464	0.0710	45.3
MOGP model II	3.1418	3.4182	3.2693	0.0900	45.2
FE model	3.3384	3.3963	3.3703	0.0185	82845.7

Table 7
Comparison of the results obtained using different simulation models in the parameter identification process.

Model	E_M (GPa)	E_K (GPa)	η_M (GP·year)	η_K (GP·year)	*RMSE_fitted* (mm)	*RMSE_predicted* (mm)
MOGP model I	3.46	3.51	1.75	80.16	0.2331	0.2007
MOGP model II	3.35	3.52	1.75	88.41	0.2255	0.1780
FE model	3.42	3.46	1.56	89.37	0.2120	0.1803

$$aR^2 = \frac{1}{T}\sum_{j=1}^{T}\frac{\left[\sum_{i=1}^{N}(f_{ij}-\bar{f}_j)(y_{ij}-\bar{y}_j)\right]^2}{\sum_{i=1}^{N}(f_{ij}-\bar{f}_j)^2\sum_{i=1}^{N}(y_{ij}-\bar{y}_j)^2} \tag{19}$$

where N is the number of samples; T is the number of the output data; y is observed displacement values of FE simulation; $\bar{y}$ is the average of observed values; f denotes the predicted displacement values; $\bar{f}$denotes the average of predicted values. Here, smaller values of *aRMSE*, *MAXE* and *aMAE* and a larger value of aR^2 reflect better model performance.

3.3. Optimization procedure

The parameters to be determined are viscoelastic parameters of the

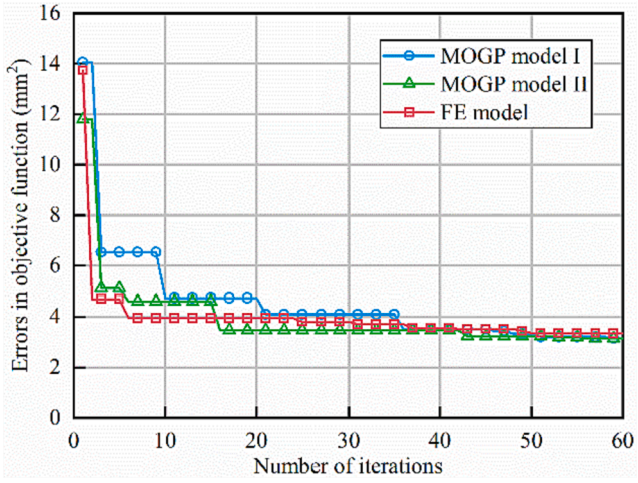

Fig. 9. Convergence curves recorded in the parameter identification process.

Burgers model which is employed to describe the constitutive relationship of the dam foundation. For consistency, the parameters of the constitutive model are recorded as a variable set **X**:

$$\mathbf{X} = [x_1, x_2, \cdots, x_d]^T \tag{20}$$

where x_i $(i = 1, 2, \cdots, d)$ represents the unknown parameters.

The inverse analysis problem can be formulated to find the optimized parameters by adjusting the variable set **X** until the calculated displacements of the surrogate model match the monitoring data in a least-squares fashion. The objective function is defined as follows:

$$F(\mathbf{X}) = \frac{1}{T}\sum_{t=1}^{T}(y_t - y'_t)^2 \tag{21}$$

where y_t and y'_t $(t = 1, 2, .., T)$ represent the monitoring and calculated displacements, respectively; T is the number of observations.

Bound constraints are introduced to the variables:

$$x_{li} \le x_i \le x_{ui} (i = 1, 2, \cdots, d) \tag{22}$$

wherex_{li} and x_{ui} are the lower and upper bounds of the i-th parameter, respectively.

In this study, the multi-verse optimizer (MVO) [45] is used in the context of an indirect inverse analysis method for parameter identification. A solution (a set of unknown viscoelastic parameters) is represented by a universe in MVO, a variable/parameter in the solution corresponds to an object in the universe, and the fitness value of the solution (value of the objective function) is indicated by the inflation rate of the universe.

A brief optimization process of MVO is described in Algorithm 1. The universe set U is defined as:

$$\mathbf{U} = \begin{bmatrix} U_1 \\ U_2 \\ \vdots \\ U_m \end{bmatrix} = \begin{bmatrix} x_1^{(1)} & x_2^{(1)} & \cdots & x_d^{(1)} \\ x_1^{(2)} & x_2^{(2)} & \cdots & x_d^{(2)} \\ \vdots & \vdots & \vdots & \vdots \\ x_1^{(m)} & x_2^{(m)} & \cdots & x_d^{(m)} \end{bmatrix} \tag{23}$$

where d is the number of objects (unknown viscoelastic parameters) and m is the number of universes (candidate solutions).

The mathematical model of this algorithm depends on Eqs. and which are described as follows:

$$x_j^{(i)} = \begin{cases} x_j^{(k)}, & r_1 < NI(U_i) \\ x_j^{(k)}, & r_1 \geqslant NI(U_i) \end{cases} \tag{24}$$

where $x_j^{(i)}$ represents the j-th variable of the i-th universe; $x_j^{(k)}$ represents the j-th variable of the k-th universe which selected by a roulette wheel selection mechanism; U_i denotes the i-th universe and $NI(U_i)$ is the normalized inflation rate (fitness value) of U_i; r_1 is a random number in the range of [0,1].

The evolution of universes also follows:

$$x_j^{(i)} = \begin{cases} \begin{cases} X_j + TDR^*\left((ub_j - lb_j)^* r_4 + lb_j\right), r_3 < 0.5 \\ X_j - TDR^*\left((ub_j - lb_j)^* r_4 + lb_j\right), r_3 \geq 0.5 \end{cases} & r_2 < WEP \\ x_j^{(i)} & r_2 \geq WEP \end{cases} \tag{25}$$

where X_j denotes the j-th variables of the best universe formed so far; $lb_j$and ub_j denotes the lower and upper boundaries of the j-th variable; r_2, r_4,and r_4 are random numbers in the range of [0,1].

There are two adaptive coefficients in the MVO: the wormhole existence probability (WEP) and the travelling distance rate (TDR), which are expressed as follows:

$$\mathrm{WEP} = \mathrm{WEP}_{\min} + l^*\left(\frac{\mathrm{WEP}_{\max} - \mathrm{WEP}_{\min}}{L}\right) \tag{26}$$

$$\mathrm{TDR} = 1 - \frac{l^{1/b}}{L^{1/b}} \tag{27}$$

where $\mathrm{WEP}_{\min}$ is the minimum value which is ordinarily set to 0.2; $\mathrm{WEP}_{\max}$is the maximum value which is ordinarily set to 1; $l$and L represent the current iteration number and the maximum iteration number, respectively; b indicates the exploitation factor which is ordinarily set to 6 [45].

Algorithm 1 Multi-Verse Optimizer

Input: Ranges of viscoelastic parameters, Number of Universes, Number of iterations
Output: Best_Universe
Function MVO
1:**for** each Universe i
2:Initialize positions for Universe i, coefficients WEP and TDR
3:Evaluate the inflation rate of Universe i
4:**end for**
5: Record Best_Universe which has the minimum inflation rate
6: **while** iteration < max_iteration
7: **for** each Universe i
8: Update the position of Universe i ▸ Apply the Eqs. (25) and (26)
9: **if** Inflation_rate(Ui) < Best_Universe_Inflation_rate
10: Best_Universe = Universe i
11: **end if**
12: **end for**
13: Update WEP and TDR ▸ Apply the Eqs. (26) and (27)
14:**end while**
15:return Best_Universe
end function

4. Case study

In this section, a series of tests and analyses are performed on the dam section #3 (introduced in Section 2) to verify the feasibility of the proposed inversion framework based on the MOGP surrogate model. In addition, some suggestions are provided on how to build a surrogate model efficiently and accurately in similar projects.

4.1. Sensitivity analysis

Before generating FE simulation data based on DOE samples, a sensitivity study of the mechanical parameters is conducted using the orthogonal test method [46,47]. The obtained information helps to verify the rationality of the selected mechanical parameters and their search ranges in the inverse analysis (i.e. the parameters and ranges selected to train a surrogate model). The orthogonal test method is a kind of designing method based on mathematical statistics and the orthogonality principle. It involves selecting representative points from a large number of experimental points and analysing them in multifactor experiments using an

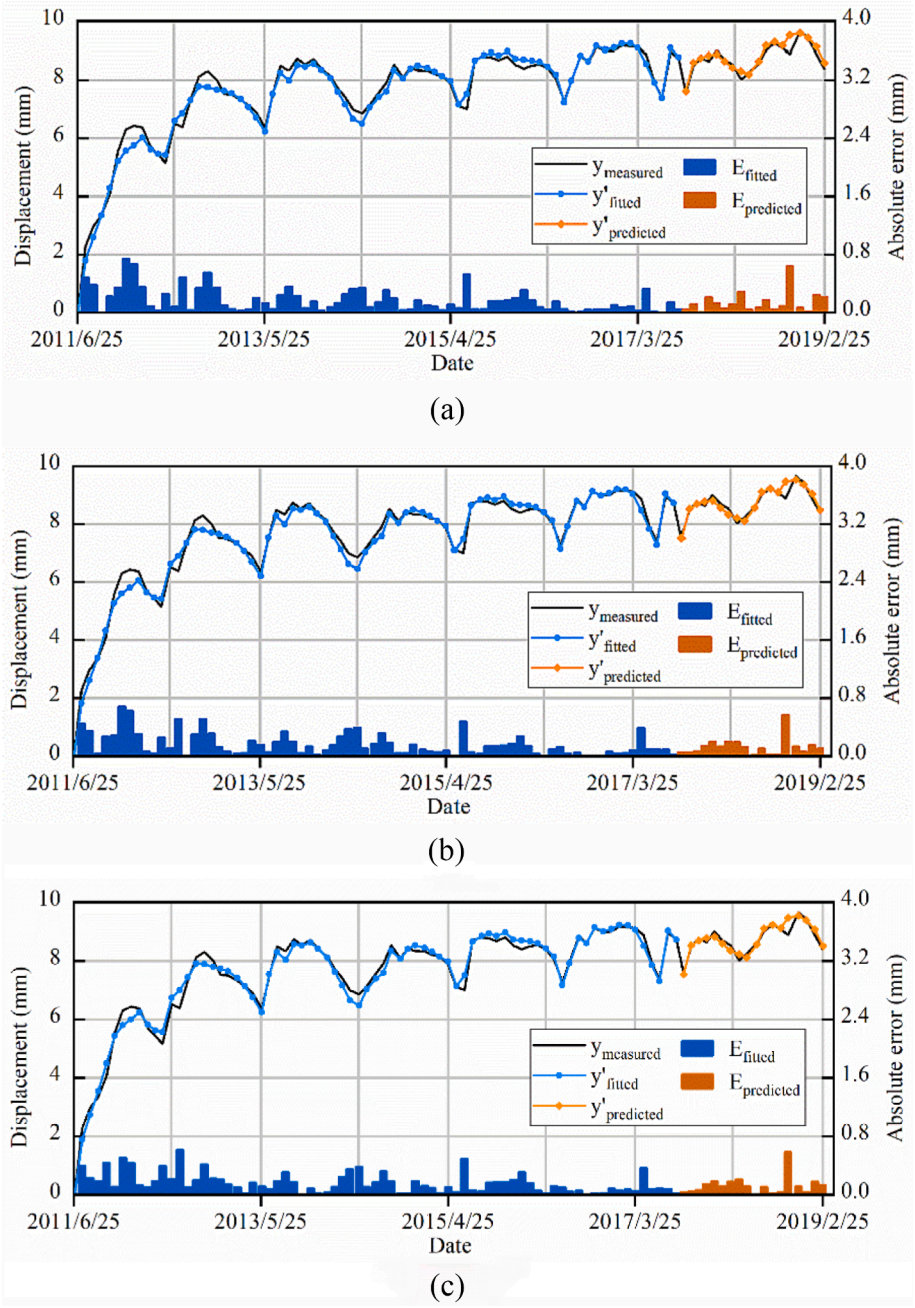

Fig. 10. Fitted and predicted displacements based on the parameters identified via (a) MOGP model I, (b) MOGP model II, and (c) FE model.

orthogonal table [48].

In this study, the dam foundation is simulated by the Burgers model and four viscoelastic parameters considered in the orthogonal test are taken as: $E_M \in [1\text{GPa}, 5\text{GPa}]$, $E_K \in [1\text{GPa}, 5\text{GPa}]$, $\eta_M \in [50\text{GPa·year}, 150\text{GPa·year}]$ and $\eta_K \in [1\text{GPa·year}, 5\text{GPa·year}]$. The other mechanical parameters are taken as constant values and are described below. The dam body was constructed of C15 roller compacted concrete and are simulated by the elastic model. According to tests, the density, Young's modulus and Poisson ratio of the dam body are taken as 2.4 g/cm^3, 23 GPa and 0.167, respectively. Moreover, it is already verified that the load–displacement response of the concrete dam is not highly influenced by the Poisson ratio [14], thus the Poisson ratio of the foundation is taken as 0.25.

For four factors, where each factor is varied in three levels, the orthogonal test table of $L_9(3^4)$ is established (Table 2). A total of nine mixes are tested, and the resulting value of the objective function $F(X)$ (Eq. (21)) are listed in Table 2, where the observation times of the objective function is taken as $T = 93$ in this case.

The results of sensitivity analysis are outlined in Table 3, where K_1, K_2 and K_3 represent mean values of three levels, and R refers to the result of the extreme analysis. According to the orthogonal test theory, the factor with a larger R is more important than other factors [49]. It is observed that the scattered intervals of the four factors are similar in general, although there are some differences. The most sensitive factor is E_K followed by E_M, η_K and η_M. The results indicate the selected four parameters and their search ranges are rational in the inverse analysis.

4.2. Performance evaluation of the MOGP model

This work puts emphasis on how to efficiently establish a reliable surrogate model in an accurate and computationally-efficient manner. In this subsection, three tests are conducted to investigate the impact of sample size, parameter range and output quantity on the performance of the MOGP model.

4.2.1. Impact of the sample size

In this part, we investigate which size of training data is better for establishing the MOGP surrogate model. The Latin hypercube sampling (LHS) method is applied to uniformly generate N pairs of viscoelastic parameter samples within their ranges. These samples will be transferred to the FE program to calculate the corresponding displacement responses of the measuring point (93 output observations in total). After all the samples are calculated, an inputs-outputs dataset $D = [X, Y]$ can be obtained, which are assigned as the training set for MOGP training. In addition, another N pairs of viscoelastic parameter samples are randomly generated within the same ranges, and the obtained dataset $D_* = [X_*, Y_*]$ are assigned as the testing set to test the performance of trained MOGP. Each test instance is repeated ten times independently, and in each test instance, we re-randomise the samples.

The average and standard deviation of the performance criterion values in the training and testing stages, as well as the computational time, are listed in Table 4 and Table 5. Typically, the relationship between the average/standard deviation of *aRSME* and the sample size is plotted in Fig. 5. When the sample size is less than 50, the *aRSME* in the testing stage is more than five times that obtained in the training stage. It seems that the model is overfitting when the sample size is too small. As presented in Table 4 and Fig. 5(a), with the increase of the sample size, the MOGP model can yield better predictions. However, when the sample size is more than 80, the *aRSME* increases again both in the testing and training stages. When the sample size is set between 250 and 1000, *aRSME* converges to a constant value of 1.5 mm. It seems that a large size of samples also causes some learning artefacts. We will investigate and explain this phenomenon later. From a comprehensive perspective, the training size of 70–100 is suitable for modelling. Additionally, it can also be observed in Table 5 and Fig. 5(b) that the standard deviation of training/test errors are small when the sample size is set to 70–100.

4.2.2. Impact of the sample parameter ranges

In this part, we compare the performances of surrogate models based on samples generated in different parameter ranges. The parameter range is expanded to twice the original range: $E_M \in [1\text{GPa}, 10\text{GPa}]$, $E_K \in [1\text{GPa}, 10\text{GPa}]$, $\eta_M \in [20\text{GPa·year}, 200\text{GPa·year}]$, and $\eta_K \in [1\text{GPa·year}, 10\text{GPa·year}]$. Fig. 6 illustrates the corresponding average and standard deviation of *aRSME* of the newly established MOGP model in ten test instances. It turns out that the overall *aRSME* in this example is slightly larger than that of the previous one, which can be considered reasonable since the range of the input–output dataset has been expanded. By comparing Fig. 5 and Fig. 6, it can be seen that the *aRMSE* curves of the two cases have similar laws. This means that in the case of the expanded parameter range setting, the sample size of 70–100 in this case study is sufficient to construct an accurate and reliable surrogate model.

4.2.3. Impact of the output quantity

In the aforementioned test instances, the output data includes a series of 93 displacement observations. In this part, the performance of the MOGP model with different output quantities is examined. Based on the previous cases, the first 1/3 and 2/3 displacement observations are selected as the output of the surrogate model (the output quantity is 30 and 60, respectively), and four additional test instances are added for different parameter ranges and output quantities. Fig. 7 shows the representative metrics (average of *aRSME*) of the four instances. It can be seen that the law of the *aRMSE* curve is similar when we set different initial conditions.

4.2.4. Validation and discussion

To further prove the validity of the MOGP model, as well as to interpret the obtained model accuracy curve, some relevant analyses are performed. The results of the MOGP model based on 100 training samples are taken as an example here. The training samples are generated from the original parameter range.

After learning with 100 training samples, the trained MOGP model is tested with another 100 testing samples. Since the samples are randomly generated, the output data are ordered from minimum to maximum to make it more intuitive. Each output sample is a displacement time series with 93 observations, thus a matrix with the size of 100×93 are generated. Fig. 8 shows the response surface of the FE model and MOGP model, as well as the estimation error between the FE model and the MOGP model. It turns out that the predicted results of the MOGP model are close to the FE model, although there are some deviations at the boundary. For most points, the error between FE model and MOGP model is small, where 60% of the errors are lower than 0.1 mm, and 80% of the errors are lower than 0.3 mm. However, the MOGP model has poor performance at the edge, and the errors of some points at the boundary are up to 4 mm.

The results of different sample sizes are also analysed. It is found that the prediction accuracy of the MOGP model in the main interval is still good with the increase of sample size. However, with a larger sample size, more points will fall near the edges (close to the boundary), leading to a larger overall *aRMSE*. Since the actual values of measurements fall within the main interval of the surrogate model, therefore, the MOGP model can replace the FE model in the inverse analysis.

As a result, it is recommended using 70–100 samples to train a surrogate model for this dam case. The calculation results can meet the requirements of prediction accuracy, model reliability and efficiency simultaneously. For similar dam cases, we can perform some initial tests to find out the lower bound on the sample size suitable for learning. In addition, it is recommended performing some preliminary evaluation before training the surrogate model, which can avoid the actual monitoring data falling near the boundary of the training samples.

4.3. Parameter identification and physics-based model calibration

In this subsection, MVO is employed to identify the viscoelastic parameters of the dam foundation with the use of the surrogate model. Two surrogate models are established: MOGP model I adopts the training samples generated from the original parameter range mentioned in Section 5.1, and MOGP model II adopts the samples generated from the extended parameter range mentioned in 5.2.2. The output of both models is a series of 75 displacement observations (80% of the total observations). The remaining 20% of observations are used to calibrate the identified parameters. We adopt 100 samples to train the MOGP surrogate models, and we also test the performance of the models to ensure that they could meet the accuracy requirements.

From experience, the population size (the number of universes) is set to 20 and the maximum number of iterations is set to 60 in the MVO. The search intervals are set as $E_M \in [1\text{GPa}, 5\text{GPa}]$, $E_K \in [1\text{GPa}, 5\text{GPa}]$, $\eta_M \in [50\text{GPa·year}, 150\text{GPa·year}]$ and $\eta_K \in [1\text{GPa·year}, 5\text{GPa·year}]$. The internal parameter setting of the MVO has been explained and described in Section 3.3.

The optimization is executed in parallel on a machine with 16-core 2.10 GHz Intel Xeon Silver 4110 CPU and 48G RAM, running Windows 10. We compare the results obtained using two MOGP models and the FE model. Each test instance is repeated five times independently, and the minimum, maximum, average and standard deviation of the objective function (Eq. (21)) are listed in Table 6. As can be seen from Table 6, the optimal objective-function value of the MOGP model is similar to that in the FE model case, which also reflects the trained MOGP model is accurate and reliable.

The best results in the identification process of each model are presented in Table 7 and the corresponding convergence curves recorded are shown in Fig. 9. We substitute the identified parameters into the FE program for calibration (where the fitted/predicted results have a physical meaning). Fig. 10 shows the fitted and predicted displacements based on the parameters identified via three different simulation models, and the performance evaluation results (*RMSE_fitted* and *RMSE_predicted*) are given in Table 7. It is observed in Fig. 10 that the fitted and predicted process lines of the three models are all close to the measured process line. As presented in Table 7, the evaluation results obtained based on the two surrogate models are very close to those obtained by the FE model, indicating the rationality of the inversion results.

The results presented above prove that the proposed inversion method based on the MOGP surrogate model applies to the inverse problem dealt with in this case study. It is worth mentioning that the use of the surrogate model can significantly reduce the burden of FE calculations (see Table 6). The inverse analysis of long-term viscoelastic monitoring data suffers a high computation cost because a great many FE iterations are required in the optimization loop. Therefore, it is not economical to directly implement the FE model in the optimization process, especially for large-scale engineering structures with complex constitutive relationships. In the proposed method, we only need to calculate a small amount of FE samples in advance to build a surrogate model, and the calculation cost of implementing the surrogate model in the optimization process is low. As in this case study, we can save about 90% of the time overall. Moreover, the trained surrogate model is also suitable for embedding in online monitoring platforms to provide online feedback.

5. Conclusion

Inverse analysis is an effective technique to identify mechanical parameters of dam system and to calibrate physics-based monitoring models. In contrast to traditional inverse analysis methods which place the finite element computation inside the optimization loop, this article proposes a multi-output surrogate model approach. This approach not only achieves accurate estimation of mechanical parameters but also greatly improves computational efficiency.

The proposed inversion method is demonstrated on a gravity dam example. The following concluding remarks can be made:

(1) MOGP modelling technique is used to approximate the load–displacement relationship of the finite element model in the creep regime. A series of time-dependent viscoelastic displacement responses of the dam foundation can be quickly computed with the given intrinsic mechanical parameters, which greatly improves the computational efficiency at a low precision loss.

(2) The sensitivity of the training sample size, parameter range and output quantity of the MOGP model is investigated to establish a proficient surrogate model with as few samples as possible. It is recommended that 70–100 samples be used to train a surrogate model for this dam example. For similar dam projects, it is recommended to perform some initial tests to find out the lower bound of a suitable learning sample size.

(3) The viscoelastic parameters of the Burgers model are identified using the MOGP surrogate model and a *meta*-heuristic optimization algorithm called MVO. The results illustrate that the identified properties allow predictions on dam displacement to be consistent with the long-term monitoring data. It is concluded that the proposed inversion method reasonably applies to parameter identification problems of concrete dams.

(4) In this study, the inverse analysis is carried out in a deterministic manner. In future work, we plan to investigate a probabilistic inversion method based on Bayes' theorem to estimate the posterior distribution of viscoelastic parameters by incorporating the uncertainty of obtained information.

CRediT authorship contribution statement

Chaoning Lin: Conceptualization, Data curation, Formal analysis, Methodology, Software, Writing – original draft. **Tongchun Li:** Funding acquisition, Project administration, Resources, Supervision. **Siyu Chen:** Methodology, Visualization, Investigation, Software, Writing – review & editing. **Li Yuan:** Validation, Formal analysis. **P.H.A.J.M. van Gelder:** Writing – review & editing, Supervision. **Neil Yorke-Smith:** Visualization, Writing – review & editing, Supervision.

Declaration of Competing Interest

The authors declare that they have no known competing financial interests or personal relationships that could have appeared to influence the work reported in this paper.

Acknowledgements

This research was greatly supported by National Key Research and Development Plan (No. 2018YFC0407102); Project of the research on long term monitoring and safety evaluation of concrete dams based on BIM (DJ-ZDXM-2018-02); and China Scholarship Council (CSC No. 201906710131).

References

[1] De Sortis A, Paoliani P. Statistical analysis and structural identification in concrete dam monitoring. Eng Struct 2007;29:110–20.
[2] Hariri-Ardebili MA. Risk, Reliability, Resilience (R-3) and beyond in dam engineering: A state-of-the-art review. Int J Disaster Risk Reduct 2018;31:806–31.
[3] Hariri-Ardebili MA, Sudret B. Polynomial chaos expansion for uncertainty quantification of dam engineering problems. Eng Struct 2020;203:109631.
[4] Hariri-Ardebili MA, Salazar F. Engaging soft computing in material and modeling uncertainty quantification of dam engineering problems. Soft Comput 2019;24:11583–604.
[5] Bukenya P, Moyo P, Beushausen H, Oosthuizen C. Health monitoring of concrete dams: a literature review. Journal of Civil Structural Health Monitoring 2014;4:235–44.
[6] Chen S, Gu C, Lin C, Hariri-Ardebili MA. Prediction of Arch Dam Deformation via Correlated Multi-Target Stacking. Appl Math Model 2021;91:1175–93.
[7] Salazar F, Morán R, Toledo MÁ, Oñate E. Data-based models for the prediction of dam behaviour: a review and some methodological considerations. Arch Comput Methods Eng 2017;24:1–21.
[8] Hellgren R, Malm R, Ansell A. Performance of data-based models for early detection of damage in concrete dams. Struct Infrastruct Eng 2020;17:275–89.
[9] Maier G, Ardito R, Fedele R. Inverse Analysis Problems in Structural Engineering of Concrete Dams. Proceedings of the Sixth World Congress on Computational Mechanics in Conjunction with the Second Asian-Pacific Congress on Computational Mechanics. Beijing, China.2004.
[10] Toromanovic J, Mattsson H, Knutsson S, Laue J. Parameter identification for an embankment dam using noisy field data. Geotechnical Engineering 2020;1–42.
[11] Yu Y, Liu X, Wang E, Fang K, Huang L. Dam safety evaluation based on multiple linear regression and numerical simulation. Rock Mech Rock Eng 2018;51:2451–67.
[12] Gu H, Wu Z, Huang X, Song J. Zoning Modulus Inversion Method for Concrete Dams Based on Chaos Genetic Optimization Algorithm. Mathematical Problems in Engineering 2015;1–9.
[13] Dou S, Li J, Kang F. Parameter identification of concrete dams using swarm intelligence algorithm. Engineering Computations 2017;34:2358–78.
[14] Kang F, Li J, Xu Q. Structural inverse analysis by hybrid simplex artificial bee colony algorithms. Comput Struct 2009;87:861–70.
[15] Labibzadeh M, Khayat M. Heterogeneous and anisotropic long-term concrete damage of the dez arch dam using thermal inverse analysis. Inverse Prob Sci Eng 2016;24:1495–509.
[16] Song J, Gu C, Su H, Gu H, Huang X. Observed displacement data-based identification method of structural damage in concrete dam. Eng Fail Anal 2016;66:202–11.
[17] Lin C, Li T, Liu X, Zhao L, Chen S, Qi H. A deformation separation method for gravity dam body and foundation based on the observed displacements. Structural Control and Health Monitoring 2019;26:e2304.
[18] Su H, Wen Z, Zhang S, Tian S. Method for Choosing the Optimal Resource in Back-Analysis for Multiple Material Parameters of a Dam and Its Foundation. J Comput Civil Eng 2016;30:4015060.
[19] Papadopoulos V, Soimiris G, Giovanis D, Papadrakakis M. A neural network-based surrogate model for carbon nanotubes with geometric nonlinearities. Comput Methods Appl Mech Eng 2018;328:411–30.

[20] Xiang H, Li Y, Liao H, Li C. An adaptive surrogate model based on support vector regression and its application to the optimization of railway wind barriers. Struct Multidiscip Optim 2017;55:701–13.
[21] Cheng K, Lu Z, Ling C, Zhou S. Surrogate-assisted global sensitivity analysis: an overview. Structural and Multidiplinary Optimization 2020;61:1187–213.
[22] Hariri-Ardebili MA, Mahdavi G, Abdollahi A, Amini A. An RF-PCE Hybrid Surrogate Model for Sensitivity Analysis of Dams. Water 2021;13:302.
[23] Fedele R, Maier G, Miller B. Health assessment of concrete dams by overall inverse analyses and neural networks. Int J Fract 2006;137:151–72.
[24] Dou S, Li J, Kang F. Health diagnosis of concrete dams using hybrid FWA with RBF-based surrogate model. Water Sci Eng 2019;12:188–95.
[25] Sevieri G, Andreini M, De Falco A, Matthies HG. Concrete gravity dams model parameters updating using static measurements. Eng Struct 2019;196:109231.
[26] Liu C, Gu C, Chen B. Zoned elasticity modulus inversion analysis method of a high arch dam based on unconstrained Lagrange support vector regression (support vector regression arch dam). Engineering with Computers 2016;33:443–56.
[27] Williams CK, Rasmussen CE. Gaussian processes for machine learning: Cambridge, MA. USA: MIT Press; 2006.
[28] Lin C, Li T, Chen S, Liu X, Lin C, Liang S. Gaussian process regression-based forecasting model of dam deformation. Neural Comput Appl 2019;31:8503–18.
[29] Du A, Padgett JE. Investigation of multivariate seismic surrogate demand modeling for multi-response structural systems. Eng Struct 2020;207:110210.
[30] Olalusi OB, Awoyera P. Shear capacity prediction of slender reinforced concrete structures with steel fibers using machine learning. Eng Struct 2021;227.
[31] Kang F, Li J. Displacement Model for Concrete Dam Safety Monitoring via Gaussian Process Regression Considering Extreme Air Temperature. J Struct Eng 2020;146:05019001.
[32] Kang F, Xu B, Li J, Zhao S. Slope stability evaluation using Gaussian processes with various covariance functions. Appl Soft Comput 2017;60:387–96.
[33] Zhou T, Peng Y. Kernel principal component analysis-based Gaussian process regression modelling for high-dimensional reliability analysis. Comput Struct 2020;241:106358.
[34] Wan H, Ren W. A residual-based Gaussian process model framework for finite element model updating. Comput Struct 2015;156:149–59.
[35] Lu J, Zhan Z, Apley DW, Chen W. Uncertainty propagation of frequency response functions using a multi-output Gaussian Process model. Comput Struct 2019;217:1–17.
[36] Álvarez MA, Luengo D, Titsias MK, Lawrence ND. Efficient multioutput gaussian processes through variational inducing kernels. Journal of Machine Learning Research 2010;9:25–32.
[37] Duong PLT, Park H, Raghavan N. Application of multi-output Gaussian process regression for remaining useful life prediction of light emitting diodes. Microelectron Reliab 2018;88:80–4.
[38] Liu H, Cai J, Ong Y-S. Remarks on multi-output Gaussian process regression. Knowl-Based Syst 2018;144:102–21.
[39] Lin C, Li T, Chen S, Lin C, Liu X, Gao L, et al. Structural identification in long-term deformation characteristic of dam foundation using meta-heuristic optimization techniques. Adv Eng Softw 2020;148:102870.
[40] Zhang Y, Xu W, Shao J, Zhao H, Wang W. Experimental investigation of creep behavior of clastic rock in Xiangjiaba Hydropower Project. Water Sci Eng 2015;8:55–62.
[41] Fernandez-Merodo JA, Castellanza R, Mabssout M, Pastor M, Parma M. Coupling transport of chemical species and damage of bonded geomaterials. Comput Geotech 2007;34:200–15.
[42] Ciantia MO, Castellanza R, Fernandez Merodo JA, Hueckel T. A multiscale approach for evaluating the failure condition of calcarenite structures subject to environmental loads. International Symposium on Geomechanics from Micro to Macro: Taylor & Francis; 2015.
[43] Stein M. Large sample properties of simulations using Latin hypercube sampling. Technometrics 1987;29:143–51.
[44] Kong D, Chen Y, Li N. Gaussian process regression for tool wear prediction. Mech Syst Sig Process 2018;104:556–74.
[45] Mirjalili S, Mirjalili SM, Hatamlou A. Multi-Verse Optimizer: a nature-inspired algorithm for global optimization. Neural Comput Appl 2016;27:495–513.
[46] Li Y, She L, Wen L, Zhang Q. Sensitivity analysis of drilling parameters in rock rotary drilling process based on orthogonal test method. Eng Geol 2020;105576.
[47] Li X, Hao J. Orthogonal test design for optimization of synthesis of super early strength anchoring material. Constr Build Mater 2018;181:42–8.
[48] Zhang Q, Leung YW. An orthogonal genetic algorithm for multimedia multicast routing. IEEE Trans Evol Comput 1999;3:53–62.
[49] Zhang Z, Fang H, Yan H, Jiang Z, Zheng J, Gan Z. Influencing factors of GaN growth uniformity through orthogonal test analysis. Appl Therm Eng 2015;91:53–61.